

Assessing the Effects of Tidal Energy Converter Array Size on Hydrodynamics of Ria Formosa (Portugal)

Eduardo González-Gorbeña^{#1}, André Pacheco^{#2}, Theocharis A. Plomaritis^{#3}, Cláudia Sequeira^{#4}

[#] Centre for Marine and Environmental Research (CIMA), Universidade do Algarve (UALg),

Edifício 7, Campus de Gambelas Faro, 8005-139, Portugal

¹egeisenmann@ualg.pt

²ampacheco@ualg.pt

³tplomaritis@ualg.pt

⁴cdsequeira@ualg.pt

Abstract— This paper investigates the effects of Tidal Energy Converter (TEC) array size at a tidal channel on flood/ebb discharges at multi-inlet coastal lagoon by applying numerical modelling. The paper presents a case study for the Faro-Olhão inlet in the Ria Formosa (Portugal), a potential site for tidal in-stream energy extraction. Arrays of up to 11 rows with 5 TECs each were studied to assess impacts on inlets discharges changes. For the particular cases assessed the results show that tidal energy extraction will have a greater impact on Ancão and Armona inlets discharges together with the Faro-Olhão inlet. Future work is directed to include impacts on sediment dynamics and optimise TEC array size as a function of multiple design variables subject to environmental constraints.

Keywords— Tidal stream energy, hydrodynamic modelling, flood/ebb discharges impact, array size, multi-inlet coastal lagoon.

I. INTRODUCTION

Tidal stream energy harvesting consists in extracting part of the kinetic energy from the natural ebb/flow of coastal tidal waters to generate electricity. Tidal Energy Converters (TEC) are used for this purpose and, currently, there are numerous types of technologies being developed and tested at different readiness levels [1]. Tidal energy has the advantage of being a renewable source of energy with high density, which makes it possible to produce electricity from low flow speeds compared for example with wind energy. As a result of the gravitational fields from both the sun and the moon, combined with the earth's rotation around its axis, tidal flows are extremely predictable, and therefore simple to calculate the amount of power that can be generated at a particular time.

The tidal energy potential at shallow water estuaries and coastal lagoon systems can lead to a new generation of TEC devices based on micro generation principles, connected in arrays to produce enough energy to cover regional and/or local supply demands. Several coastal areas with estuarine characteristics at the UK, Ireland, Spain and Portugal such as Severn estuary (Wales, UK) [2], Shannon Estuary (Ireland) [3], Rias Baixas (Galicia, Spain) [4] and Ria Formosa (Algarve, Portugal) [5] are potential places for tidal energy

extraction and/or places that can be promoted as test sites for new and existent devices. However, many potential areas for TEC operation are also sensitive natural areas that are highly dynamic and hot spots of ecological richness that encompass a wide range of commercial and recreational activities. The direct consequence of installing and operating a TEC is the alteration of the hydrodynamic field of the system. As the number of TEC units increases so does the drag exerted to the flow, affecting the propagation of the tidal wave and impacting water levels and flow velocities well beyond the location of the tidal array. This modification of the hydrodynamic field can potentially translate in other environmental impacts such as: decrease tidal flooding, affect the transport and deposition of sediments, modify population distribution and dynamic of marine organisms, alter water quality, transform marine habitats and increase mixing in systems where salinity/temperature gradients are well defined [6-11].

This paper relates to the hydrodynamic modelling of tidal energy arrays using as a case study the Ria Formosa coastal lagoon (Algarve, Portugal). The purpose is to assess the effects of different TEC array sizes on the lagoon hydrodynamics, specifically with inlets discharges. Here, a floatable 1:4 scale Evopod E35 TEC rated at 35 kW from Oceanflow Energy Ltd. is used for calculations.

II. BACKGROUND

In order to ensure the commercial viability of a tidal energy project TECs are grouped in arrays. For a given tidal channel there exist an optimum number of TECs organized in rows and columns that maximises array efficiency. This optimum is related to various blockage ratios as investigated by several authors [12-19] in uniform rectangular channels using one-dimensional theoretical models based on actuator disk theory.

Obviously, when it comes to real case scenarios with complex three-dimensional flows the aforementioned models, due to their derivation assumptions, are not able to adequately represent the flow surrounding the tidal array and even less to assess its effects on the hydrodynamics of the whole system. For this purpose, numerical modelling is a useful tool to

simulate case scenarios which can provide reliable information on the influences that different tidal array schemes have on the system hydrodynamics [20,21] and therefore can be used for TEC array optimisation purposes [22,23].

For the purpose of this study, a 2-dimensional vertical averaged (2DH) hydrodynamic model has been chosen to assess the effects of TEC array size, in terms of number of turbine rows, located in the Faro-Olhão inlet in the Ria Formosa, Portugal.

III. SITE DESCRIPTION

The Ria Formosa is a multi-inlet barrier system located in southern Portugal (Fig. 1), comprising five islands, two peninsulas separated by six tidal inlets, salt marshes, sand flats and a complex network of tidal channels. The tides in the area are semi-diurnal with typical average astronomical ranges of 2.8 m for spring tides and 1.3 m for neap tides. A maximum tidal range of 3.5 m can be reached during equinoctial tides, and over 3.8 m with surge setup. Wave climate in the area is moderate (an offshore annual mean significant wave height of $H_s \sim 1$ m and peak period, T_p of 8.2 s, with storms characterized by $H_s > 3$ m). Approximately 71 % of waves approach from the W-SW, with about 23 % coming from E-SE [24]. River discharges into the lagoon are negligible, therefore, baroclinic effects are minor.

The evolution and migration of the inlets over time contributes to a great extent to the extremely dynamic character of the barrier system. Additionally, other processes such as longshore drift, overwash, aeolian dune formation, back barrier processes and artificial nourishment actions have also significantly contributed to shape the barrier islands. Several economic activities take place in the Ria Formosa such as aquaculture, salt farming, fishing, shellfish culture, shipping, mining, and tourism. These activities have local and regional importance, and the shellfish culture also assumes national impact representing 60% of the total Portuguese production. Such a congregation of different activities makes the management of the Ria Formosa a very difficult task for the region's decision-makers.

Energy from tides had been harvested before at Ria Formosa using tide mills (XII century). A recent tidal energy assessment determined for a specific cross section of the Faro-Olhão inlet a mean and maximum potential extractable power of 0.4 kW.m⁻² and 5.7 kW.m⁻², respectively [5]. This region has been selected as a representative scenario where TECs can be used to extract energy to power small communities on estuaries and coastal areas.

IV. METHODOLOGY

A. Numerical Modelling Details

1) General Model Concept: A Delft3D model of the entire Ria Formosa has been set-up and calibrated to define the extraction potential at the test case site taking into consideration both the resource (tidal energy) and the environment (consequences). Delft3D-Flow (Delft Hydraulics) is a multi-dimensional hydrodynamic (and transport)

simulation program which calculates non-steady flow and transport phenomena that result from tidal and meteorological forcing on a rectilinear or a curvilinear, boundary fitted grid. The model is a finite difference code that solves the baroclinic Navier-Stokes and transport equations under the shallow water and Boussinesq assumptions [25]. It can be used as a 3D model, or as a 2DH (vertically averaged) model, as in the present case. The hydrostatic vertical averaged shallow water equations, expressing the conservation of mass and momentum, are given in Cartesian rectangular coordinates in the horizontal plane by:

$$\frac{\partial \zeta}{\partial t} + \frac{\partial[(d+\zeta)U]}{\partial x} + \frac{\partial[(d+\zeta)V]}{\partial y} = Q \quad (1)$$

$$\begin{aligned} \frac{\partial U}{\partial t} + U \frac{\partial U}{\partial x} + V \frac{\partial U}{\partial y} - fV = \dots \\ \dots - g \frac{\partial \zeta}{\partial x} - \frac{g}{\rho_0} \int_{-d}^{\zeta} \frac{\partial \rho'}{\partial x} dz + \frac{\tau_{sx} - \tau_{bx}}{\rho_0 (d+\zeta)} + \nu_h \nabla^2 U + M_x \end{aligned} \quad (2)$$

$$\begin{aligned} \frac{\partial V}{\partial t} + U \frac{\partial V}{\partial x} + V \frac{\partial V}{\partial y} - fU = \dots \\ \dots - g \frac{\partial \zeta}{\partial y} - \frac{g}{\rho_0} \int_{-d}^{\zeta} \frac{\partial \rho'}{\partial y} dz + \frac{\tau_{sy} - \tau_{by}}{\rho_0 (d+\zeta)} + \nu_h \nabla^2 V + M_y \end{aligned}$$

where ζ is the water level above a reference plane; d is the depth below this plane; U and V are the vertically integrated velocity components in the x and y directions, respectively; Q represents the intensity of mass sources per unit area (i.e. the contributions per unit area due to the discharge or withdrawal of water, precipitation and evaporation); f is the Coriolis parameter; g is the gravitational acceleration; ν_h is the horizontal eddy viscosity coefficient; ρ_0 and ρ' are the reference and anomaly density, respectively; τ_{bx} and τ_{by} are the shear stress components at the bottom; τ_{sx} and τ_{sy} are the shear stress components at the surface; and M_x and M_y are additional source or sink of momentum terms.

2) Model Set-up: To set up the model, a curvilinear orthogonal grid in spherical coordinates has been built using the high resolution LiDAR topo-bathymetry performed on 2011, coupled with bathymetric data from the Faro Port Authority and with 2016' bathymetric surveys performed under the SCORE project. The total study domain is discretised in a 551×232 grid points in m and n direction, given a curvilinear grid resolution that varies between $\Delta x = 50$ m, $\Delta y = 30$ m and $\Delta x = 150$ m, $\Delta y = 350$ m. At the ocean boundary, the sea level is prescribed using the main tidal constituents (Table 1) by computing the tidal elevation at the boundaries at each time step. The used time step is 60 s, which, according to the Courant–Friedrichs–Levy criterion, is sufficiently small to ensure numerical stability. The spatial discretisation of the horizontal advection terms is carried out using the cyclic method, and time integration was based on the ADI method. The water levels are computed at grid cell centres and velocity components are defined at the midpoints of the grid cell faces (i.e. Arakawa-C staggered grids). Bottom

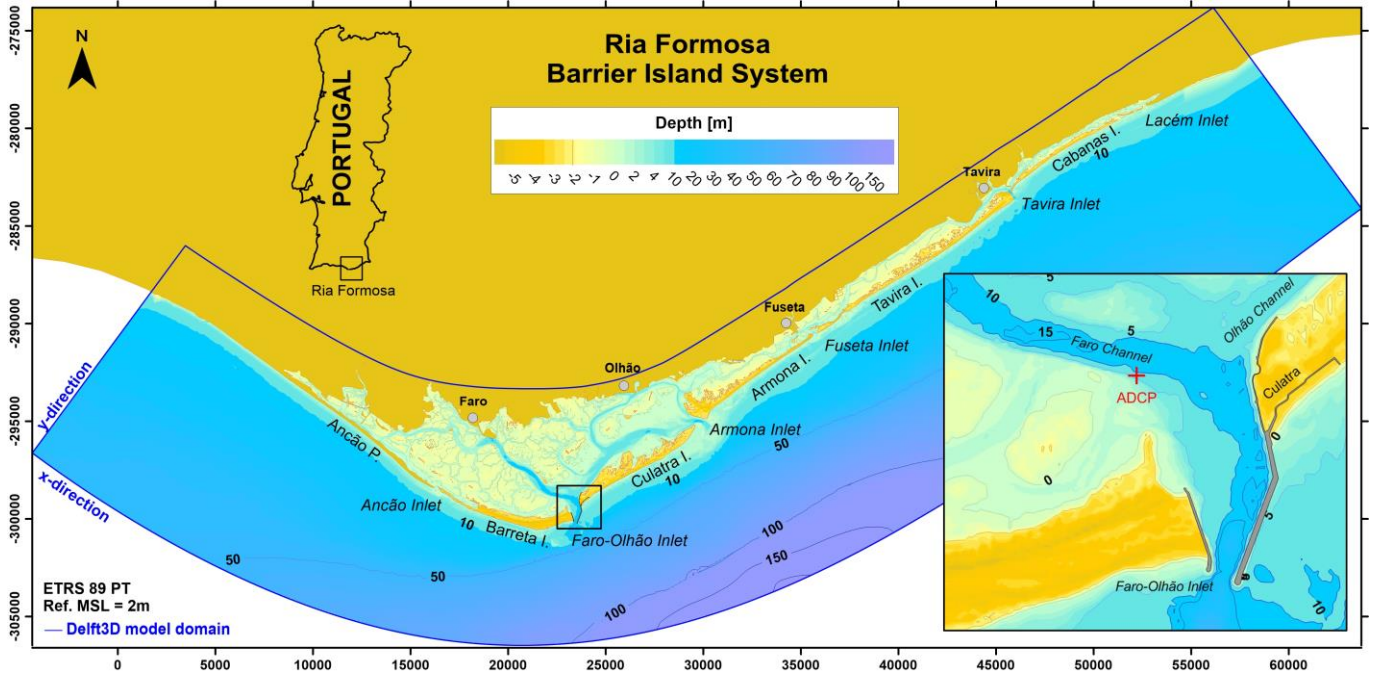


Fig. 1 Location map of the study region. Zoom rectangle shows the Faro-Olhão Inlet, the location for TEC array deployment, and the red cross shows where the ADCP was deployed. Blue line delimits model domain.

roughness has been assigned to each grid point using the Manning's formulation.

TABLE I
PRINCIPAL RIA FORMOSA TIDAL CONSTITUENTS FROM TOPEX/POSEIDON-7.2 DATA [25] [26].

Harmonic constant	Amplitude [m]	Phase [°]
M2	0.995	56.58
S2	0.365	82.57
N2	0.211	39.87
K2	0.098	78.67
K1	0.069	49.75
O1	0.058	310.45
P1	0.020	43.78
Q1	0.017	260.98
MF	0.001	261.36
MM	0.001	191.43

The simulation for calibration purposes covered the period of 16 days. i.e. 2 days of spin-up period plus 14 days of validation period (the period of interest). Calibration tests were performed to match modelled and measured velocities obtained with a bottom-mounted ADCP (Nortek Signature 1000). The ADCP was deployed at a mean water depth of 7.7 m from 03/11/2016 to 17/11/2016 using cell sizes of 0.2 m averaging every 60 s for time intervals of 300 s. The calibration involved altering grid properties (e.g. number of nodes, grid refinement, astronomical corrections), the boundary conditions (e.g. type and number of boundaries, reflection parameter alpha), the physical parameters (e.g. roughness and horizontal eddy viscosity) and the numerical parameters (e.g. smoothing time). Fig. 2 to Fig. 4 show

calibration results with reasonable agreement between observed data and model results.

To assess the model performance several statistical parameters have been calculated, these are: Bias, Standard Deviation of Residuals (SDR), Normalised Root Mean Square Error (NRMSE), Index of Agreement (IA) and Correlation Coefficient (R). Table 3 summarizes the goodness-of-fit statistics of the model. From bias we can appreciate model output tend to underestimate measured data. Northing velocity amplitudes got the worst agreement of the three variables compared with IA and R values around 0.9. Differences between measured and computed data could be related to uncertainties in bathymetric data due to a lack of accurate information of all recent dredging volumes and a grid size with a degree of refinement not enough to characterize all channels features.

$$\text{Bias} = \langle x_c - x_m \rangle \quad (3)$$

$$\text{SDR} = \left\{ \left[\langle (x_c - x_m) - (\langle x_c \rangle - \langle x_m \rangle) \rangle^2 \right] \right\}^{0.5} \quad (4)$$

$$\text{NRMSE} = \left[\langle (x_c - x_m)^2 \rangle \right]^{0.5} / |x_{m, \min} - x_{m, \max}| \quad (5)$$

$$\text{IA} = 1 - \frac{\langle (x_c - x_m)^2 \rangle}{\langle (|x_c - \langle x_c \rangle| + |x_m - \langle x_m \rangle|)^2 \rangle} \quad (6)$$

$$\text{R} = \frac{(\langle x_m x_c \rangle - \langle x_m \rangle \langle x_c \rangle)}{\left[(\langle x_m^2 \rangle - \langle x_m \rangle^2)^{0.5} (\langle x_c^2 \rangle - \langle x_c \rangle^2)^{0.5} \right]} \quad (7)$$

where x_c and x_m depict calculated and measured data, respectively, and $\langle \rangle$ stands for average values.

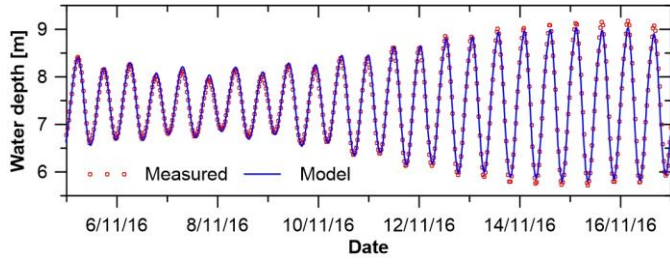


Fig. 2 Water level comparison between measured data (ADCP Nortek Signature1000) and model results (Delft3D).

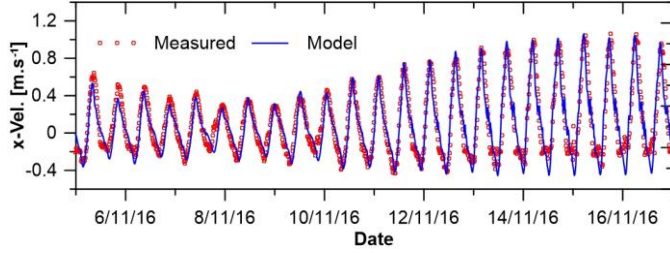


Fig. 3 Horizontal velocity component (Easting direction) comparison between measured data (ADCP Nortek Signature1000) and model results (Delft3D).

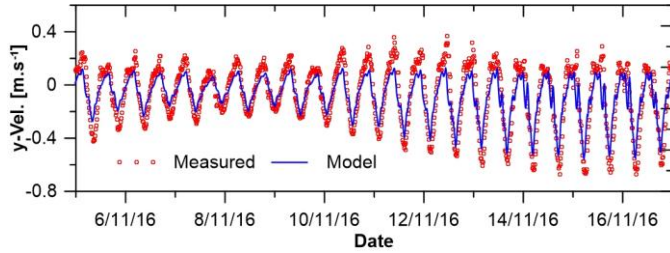


Fig. 4 Horizontal velocity component (Northing direction) comparison between measured data (ADCP Nortek Signature1000) and model results (Delft3D).

TABLE II
MODEL GOODNESS-OF-FIT STATISTICS.

Statistics	Depth	x-vel	y-vel
Bias	0.00057 [m]	-0.0163 [m.s ⁻¹]	-0.0074 [m.s ⁻¹]
SDR	0.0784 [m]	0.1295 [m]	0.1159 [m]
NRMSE	0.0074 [-]	0.0173 [-]	0.0226 [-]
IA	0.9977 [-]	0.9613 [-]	0.8983 [-]
R	0.9954 [-]	0.9291 [-]	0.9006 [-]

Fig. 5 shows a contour map of the Faro-Olhão inlet region with occurrence of tidal currents with velocities stronger than 0.7 m.s^{-1} , which is the Cut-in velocity for the Evopod E35 contemplated in this case study.

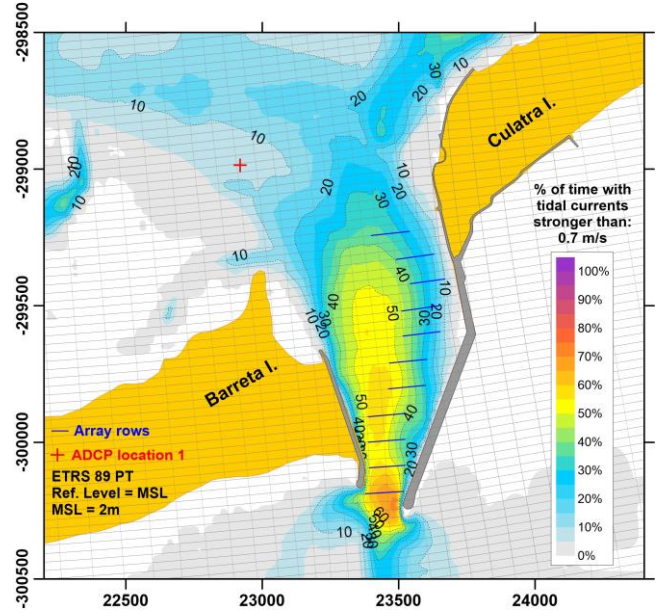


Fig. 5 Occurrence of tidal currents with velocities stronger than 0.7 m.s^{-1} for the Faro-Olhão inlet region. Red cross denotes the ADCP location and the blue lines represent TEC rows. Light grey lines represent the computational grid.

3) *Modelling tidal energy arrays*: Once the hydro-morphodynamic model is validated, the impacts of energy extraction on flow and sediment transport patterns can be simulated by enabling the sink/source momentum term of Eq. (2) to parameterize the extra loss of energy generated by a TEC array in a subgrid-scale. In Delft3D-Flow, the extra loss of energy can be parameterised using a quadratic energy loss term given by:

$$M_x = -\frac{C_{loss-u}}{\Delta x} u \sqrt{u^2 + v^2}, \quad (8)$$

$$M_y = -\frac{C_{loss-v}}{\Delta y} v \sqrt{u^2 + v^2},$$

where C_{loss} depicts de energy loss coefficient; and Δx , Δy are the cell widths in the x and y directions, respectively. The drag force, F_D , exerted in the fluid flow by an array of N -TECs devices is compose of two parts, one due to the support-structure drag, with cross-sectional area A_s , and another due to the power extraction of the turbines, with a rotor swept area of A_T with diameter D , i.e:

$$F_D = \frac{1}{2} \rho N (C_s A_s + C_T A_T) U_{in}^2 \quad (9)$$

C_s and C_T stand for the drag coefficient of the structure, and thrust coefficient of the rotor, respectively, and U_{in} is de incident flow velocity. Because F_D has force units and the momentum source term M_x has acceleration units, and to be able to relate both quantities, it is necessary to divide Eq. (9) by the control volume mass where the TEC is located, e.g. for the x-direction:

$$\frac{\rho N (C_s A_s + C_T A_T) u \sqrt{u^2 + v^2}}{2 \rho \Delta x \Delta y H} = \frac{C_{loss-u}}{\Delta x} u \sqrt{u^2 + v^2}, \quad (10)$$

where H is the water column height, $H = (d + \zeta)$, of the control cell. Solving for C_{loss} gives:

$$C_{loss-u} = \frac{N (C_s A_s + C_T A_T)}{2 \Delta y H}, \quad (11)$$

Typically, during TEC operation, thrust coefficient varies with tip speed ratio ($\beta = \omega_m R / U_{in}$, where ω_m is the angular speed), thus affecting the turbine's power coefficient, C_P [27]. As the tip speed ratio increases so do the power and thrust coefficients until the first reaches a maximum and then starts to decrease, while the latter continues increasing in value. In non-constrained flows, the optimum C_P equals the Betz Limit of 19/27 giving $C_T = 8/9$. On the other hand in-constrained flows this limit can be exceeded [28]. In channels with complex bathymetry, the free-stream flow may differ for each turbine. For the purposes of simplification, in this work is adopted a fix C_T of 0.71 and a C_S of 0.19 for all devices based on the study of [21]. Table 3 summarises the main characteristics of the device.

TABLE III
TIDAL ENERGY CONVERTER EVOPOD E35 SPECIFICATIONS.

Parameter	Value
Rotor diameter, D [m]	4.5
Length, L [m]	13
Cut-in speed, U_{ci} [$\text{m}\cdot\text{s}^{-1}$]	0.7
Rated flow speed, U_r [$\text{m}\cdot\text{s}^{-1}$]	2.3
Rated power, P_r [kW]	35
Power coefficient, C_P [-]	0.35
Thrust coefficient, C_T [-]	0.71
Swept area, A_T [m^2]	15.9
Structure drag coefficient, C_s [-]	0.19
TEC frontal area, A_s [m^2]	9.3

Array row characteristics have been defined based on Faro-Olhão channels features (i.e. geometry and water depths), results from the hydrodynamic model (i.e. occurrence of flow velocities) and TEC specifications (e.g. rotor diameter, length, etc). Each TEC row has a width of 160 m (the width of the inlet throat) incorporating 5 E35 TECs with lateral spacing of $6D$ between devices. This large lateral spacing has been adopted to allow full rotation of TECs to align with tidal current direction. First TEC row is place at the inlet throat and successive rows are placed inwards with a fix streamwise spacing between rows of $20D$ to allow a reasonable wake recovery [29]. Considering occurrence of tidal currents stronger than $0.7 \text{ m}\cdot\text{s}^{-1}$ during $\sim 25\%$ of the time or above, see Fig. 5, the maximum number of rows is set to 11 composing a maximum array length of 900 m. TEC rows are placed in regions with minimum depths of 9 m, thus array rows are not symmetrically aligned across the streamwise axis.

Operation of a TEC array will have potential impacts on aquatic environments, which can adversely impact the main economic activities carried out in the region. The magnitude of the impact will depend on TEC technology and array size. Here, we assess the effects of array size, defined in terms of number of TEC rows, on three hydrodynamic parameters, these are: cumulative flow discharges (ΔCQ_i) during a spring tide, maximum instantaneous discharges (ΔIQ_i) at each tidal inlet of Ria Formosa, and changes in the sum of the cumulative flow discharges ($\Sigma \Delta CQ_i$) for the whole system. Here, the subscript i represents each of the tidal inlets, which are shown in Fig 1. We define flood/ebb discharge as the flow that passes through an inlet cross-section. Effect on discharge is quantified calculating the percent change respect to the base case with no TECs present. A positive value being an increase in flow and a negative value being a reduction in flow. Effects on ΔCQ_i serve to identify those inlets for which larger adjustments are expected. Deviations in peak tidal current velocities are assessed through the ΔIQ_i in fixed/bed simulations. A larger ΔIQ is translated into stronger tidal currents. Changes in $\Sigma \Delta CQ_i$ for the whole system provides information of how the tidal prism is affected by array rows.

V. RESULTS AND DISCUSSION

Results retrieved for each of the 11 simulations with various tidal array sizes are compared with a baseline case scenario (i.e. without turbines), see Fig. 6 to Fig. 9.

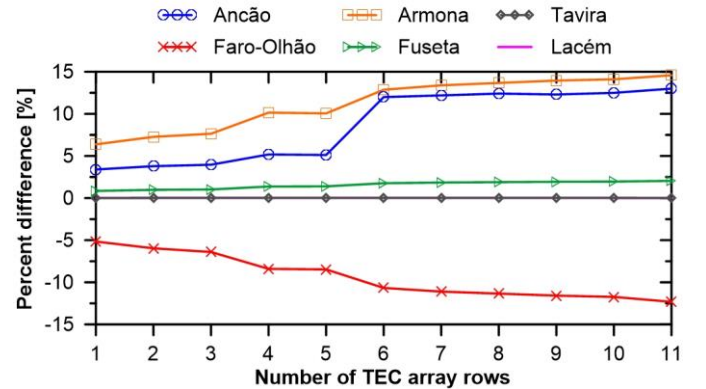


Fig. 6 Percent difference of cumulative discharges during a spring tide flood cycle for each inlet of Ria Formosa.

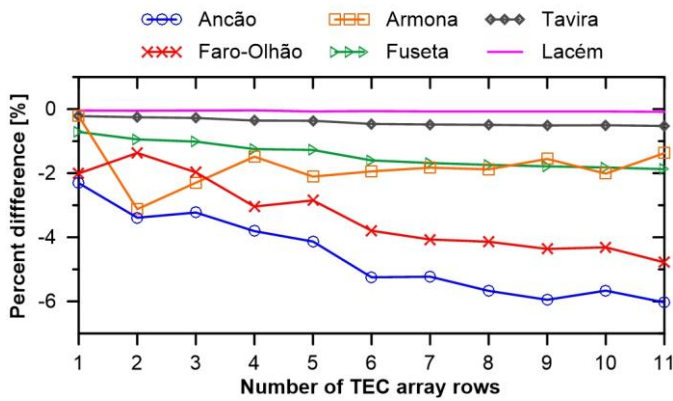


Fig. 7 Percent difference of cumulative discharges during a spring tide ebb cycle for each inlet of Ria Formosa.

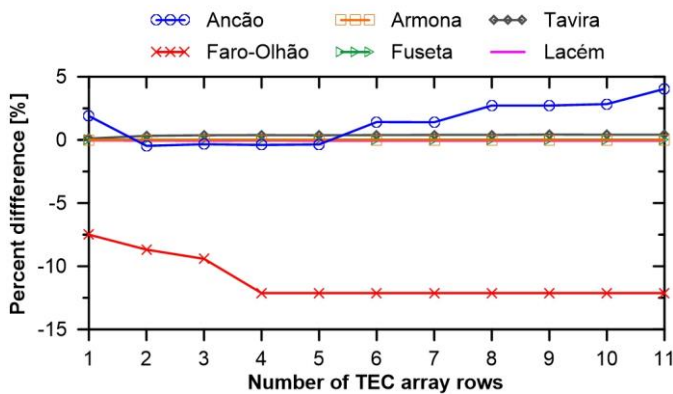


Fig. 8 Percent difference of maximum instantaneous flood discharges for each inlet of Ria Formosa.

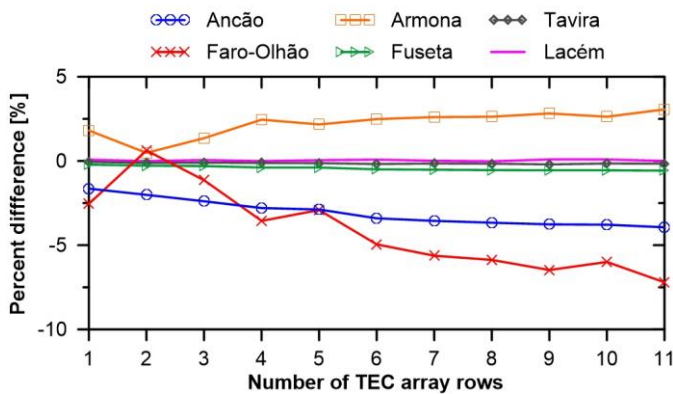


Fig. 9 Percent difference of maximum instantaneous ebb discharges for each inlet of Ria Formosa.

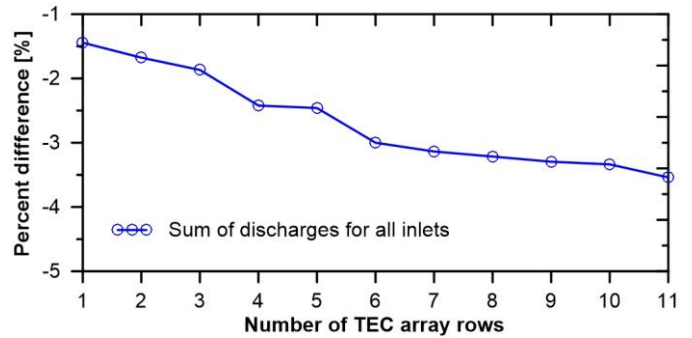


Fig. 10 Percent difference of the sum of cumulative discharges during a spring tide cycle for all 6 inlets of Ria Formosa.

Results obtained from simulations, Fig. 6 to Fig. 9, denote that Ancão and Armona inlets, located at each side of Faro-Olhão inlet, are more affected than the rest of the inlets of the lagoon system. For Ancão, Faro-Olhão and Armona inlets, cumulative spring tide discharges experiment greater alteration during flood than ebb. Moreover, while cumulative spring tide discharges in Ancão and Armona increase during flood, they decrease during ebb tide.

In general, as the number of TEC array rows increase, so do the effects on inlets discharges. As these changes in discharges do not have a smooth linear behaviour results are not easily foreseeable. The gradients of percent difference for cumulative flood discharges during a spring tide cycle, Fig. 6, for Ancão Faro-Olhão, and Armona inlets experience a large change when TEC array increase from 5 to 6 rows while changes are milder for the rest of row configurations. For the opposite case, during ebb tide (see Fig. 7) the behaviour is more irregular than during flood tide. In Ancão, cumulative discharges decrease with array size, with larger gradients for 2 and 6 rows. With 2 rows, percent differences decrease rapidly in Armona to -3 %, but discharges increase when more rows are added until reaching -1.4 % with 11 rows. In the Faro-Olhão inlet percent difference decreases for 1 to 2 rows from -2 % to -1.4% and then continuously increases until reaching a maximum of -4.8 %.

Results for percent difference of maximum instantaneous flood discharges, Fig. 8, evidence changes only for Ancão and Faro-Olhão inlets. For the Ancão inlet there is an increase in instantaneous discharges with 1 row, then becoming almost similar to the baseline case with 2 to 5 TEC rows to begin increasing up to 4 % with 11 rows. The maximum instantaneous flood discharge decrease by 7.5 % for the Faro-Olhão inlet with just a TEC array with 1 row. From 3 to 4 array rows the maximum instantaneous flood discharges reach a negative gradient of -3 % maintaining a percent difference of -12 % for the rest of the array size.

Regarding the results for percent difference of maximum instantaneous ebb discharges, Fig. 9, Ancão inlet experiences a mild linear negative increase from -1.6 % to -4 %, for 1 to 11 rows, respectively. For the Faro-Olhão inlet the placement of TEC row decrease the intensity of ebb discharges except when 2 rows are placed. In this case, maximum instantaneous discharges increase from the 1 row case in 3 %. This is because the cross section of the inlet where the second row is

positioned is larger than the first row, causing that the ebb tide accelerates at both sides of the TEC row increasing instantaneous discharges at the inlet entrance. This behaviour remains from 3 rows but with less intensity, then discharges start to weaken up to -7 %. At the Armona inlet, contrary to the Ancão inlet, instantaneous discharges increase in 1.3 %, from 1.8 % to 3.1 % for 1 row to 11 rows, respectively, but experiencing a sudden variation with 2 rows where discharges slightly decrease.

Finally, the sum of cumulative discharges during a spring tide cycle for all 6 inlets of Ria Formosa, Fig. 10, decrease with the number of TEC rows from -1.4 % to -3.5 % for 1 to 11 rows, respectively. This behaviour is in line with what is expected for hydrodynamic simulations with a fixed bottom domain. Coupling hydrodynamics with a sediment transport model will permit the assessment of dynamic equilibrium states due to TECs array presence.

VI. CONCLUSIONS

In this paper, the response of a multi-inlet coastal lagoon to several tidal stream energy array sizes located at the Faro-Olhão inlet in Ria Formosa, Portugal is investigated using hydrodynamic modelling.

The placement of one or more TECs in a tidal stream alters the fluid velocity field in relation to that in the absence of turbines. As a result, the fluid velocity field has to be determined simultaneously with the placement of a TEC array. For this purpose, numerical tools become essential to assess potential impacts of TEC arrays in aquatic environments, especially when placed in complex natural systems as is the case of multi-inlet lagoons.

This study focuses in assess the influence of TEC array size in different hydrodynamic parameters but in order to evaluate the feasibility of the tidal stream project, it is necessary to optimise the Capacity Factor of the whole array avoiding turbine rows with low efficiency. Especially in sites like the Faro-Olhão inlet where power density is not very high. For this purpose, the TEC parameterisation in the employed hydrodynamic model has to be validated, as it needs to be capable of characterising wake recovery so that the power production of turbines is estimated correctly. TEC array optimisation focus on maximising power production while minimising detrimental environmental impacts can be achieved using Surrogate Based Optimisation techniques (SBO) [30]. In the cases where time consuming numerical simulations are involved, Surrogate-Based Optimisation (SBO) revealed itself an attractive optimisation technic. In the literature, there are numerous applications of SBO techniques in various fields of knowledge [31]. Recently, SBO methods have been applied to solve the TEC array layout problem [32] aiming to maximise the overall capacity factor of the array. The SBO approach consists in approximating a mathematical function, i.e. a surrogate, to existing data or to a function that is expensive to evaluate and has no analytical form. Therefore, in cases with multiple design variable and responses this method becomes very useful to search all the variable domain

space for feasible solutions in an affordable computational time when constraints are changed.

Future work is directed towards two main objectives. The first one is related to improve the hydrodynamic model in terms of increase model resolution, perform couple sediment transport simulations, and calibrate Delft3D porous plate head loss coefficient, C_{loss} . The second objective consists in implement a TEC array surrogate-based optimisation model that: includes multiple TEC array design variables (e.g. longitudinal and lateral inter-device spacing, row positioning, etc); formulate the objective function to minimise the levelized cost of electricity, thus maximising TEC array capacity factor and; include additional environmental constraints (e.g.: water levels, morphological aspects) apart from those investigated in the present paper.

ACKNOWLEDGMENT

Eduardo G-Gorbeña has received funding for the OpTiCA project from the Marie Skłodowska-Curie Actions of the European Union's H2020-MSCA-IF-EF-RI-2016 / under REA grant agreement n° [748747]. The paper is a contribution to the SCORE project, funded by the Portuguese Foundation for Science and Technology (FCT – PTDC/AAG-TEC/1710/2014). André Pacheco was supported by the Portuguese Foundation for Science and Technology under the Portuguese Researchers' Programme 2014 entitled "Exploring new concepts for extracting energy from tides" (IF/00286/2014/CP1234).

REFERENCES

- [1] N. D. Laws, and B. P. Epps, "Hydrokinetic energy conversion: Technology, research, and outlook," *Renewable and Sustainable Energy Reviews*, vol. 57, pp. 1245-1259, 2016.
- [2] J. Xia, R. A. Falconer, and B. Lin, "Numerical model assessment of tidal stream energy resources in the Severn Estuary, UK," *Proc. IMechE Part A: J. Power and Energy*, vol. 224, pp. 969-983, 2010.
- [3] F. O'Rourke, F. Boyle, and A. Reynolds, "Ireland's tidal energy resource; An assessment of a site in the Bulls Mouth and the Shannon Estuary using measured data," *Energy Conversion and Management*, vol. 87, pp. 726-734, 2014.
- [4] R. Carballo, G. Iglesias, A. Castro, "Numerical model evaluation of tidal stream energy resources in the Ría de Muros (NW Spain)," *Renewable Energy*, vol. 34, pp. 1517-1524, 2009.
- [5] A. Pacheco and O. Ferreira, R. Carballo, and G. Iglesias, "Evaluation of the tidal stream energy production at an inlet channel coupling field data and modelling," *Energy*, vol. 71, pp. 104-117, 2014.
- [6] M. Willis, I. Masters, S. Thomas, R. Gallie, J. Loman, A. Cook, and M. Cross, "Tidal turbine deployment in the Bristol Channel: a case study," *Proceedings of the Institution of Civil Engineers-Energy*, vol. 163, np. 3, pp. 93-105, 2010.
- [7] M. Shields, M. Woolf, E. Grist, S. Kerr, A. Jackson, R. Harris, M. Bell, R. Beharie, A. Want, E. Osalusi, S. Gibb, and J. Side, "Marine Renewable Energy: the ecological implications of altering the hydrodynamics on the marine environment," *Ocean Coastal Management*, vol. 54, pp. 2-9, 2011.
- [8] SeaGen, "Environmental Monitoring Programme," Marine Current Turbines. Final Report, 2011.
- [9] C. Frid, E. Andonegi, J. Depestele, A. Judd, D. Rihan, S.I. Rogers, and E. Kenchington, "The environmental interactions of tidal and wave energy generation devices," *Environmental Impact Assessment Review*, vol. 32, no. 1, pp. 133-139, 2012.
- [10] M. Kadiri, R. Ahmadian, B. Bockelmann-Evans, W. Rauen, and R. Falconer, "A review of the potential water quality impacts of tidal

- renewable energy systems,” *Renewable and Sustainable Energy Review*, vol. 16, no. 1, pp. 329-341, 2012.
- [11] A. Copping, “Environmental effects of marine energy development around the world: Annex IV, Final Report,” Pacific Northwest National Laboratory, 2013.
- [12] C. Garrett and P. Cummins, “The power potential of tidal currents in channels,” In *Proceedings of the Royal Society of London A: Mathematical, Physical and Engineering Sciences*, vol. 461, no. 2060, pp. 2563-2572, 2005.
- [13] C. Garrett and P. Cummins, “The efficiency of a turbine in a tidal channel,” *Journal of Fluid Mechanics*, vol. 588, pp. 243-251, 2007.
- [14] R. Vennell, “Tuning turbines in a tidal channel,” *Journal of Fluid Mechanics*, vol. 663, pp. 253-267, 2010.
- [15] R. Vennell, “Tuning tidal turbines in-concert to maximise farm efficiency,” *Journal of Fluid Mechanics*, vol. 671, pp. 587-604, 2011.
- [16] T. Nishino, and R. H. Willden, “The efficiency of an array of tidal turbines partially blocking a wide channel,” *Journal of Fluid Mechanics*, vol. 708, pp. 596-606, 2012.
- [17] S. Draper, and T. Nishino, “Centred and staggered arrangements of tidal turbines,” *Journal of Fluid Mechanics*, vol. 739, pp. 72-93, 2014.
- [18] G. T. Houlby, S. Draper, and M. L. G. Oldfield, “Application of linear momentum actuator disc theory to open channel flow,” Report no. OUEL, 2296(08), 2008.
- [19] J. I. Whelan, J. M. R. Graham, and J. A. Peiro, “Free-surface and blockage correction for tidal turbines,” *Journal of Fluid Mechanics*, vol. 624, pp. 281-291, 2009.
- [20] E. González-Gorbeña, R. Y. Qassim, and P. C. Rosman, “Assessment of the tidal current energy resource in São Marcos Bay, Brazil,” *Journal of Ocean Engineering and Marine Energy*, vol. 1, no. 4, pp. 421-433, 2015.
- [21] A. Pacheco and O. Ferreira, “Hydrodynamic changes imposed by tidal energy converters on extracting energy on a real case scenario,” *Applied Energy*, vol. 180, pp. 369-385, 2016.
- [22] S.W. Funke, S.C. Kramer, M.D. Piggott, “Design optimisation and resource assessment for tidal-stream renewable energy farms using a new continuous turbine approach,” *Renewable Energy*, vol. 99, pp. 1046-1061, 2016.
- [23] N. Kurt, J. Scott, R. Jesse, J. Craig, “A framework for determining improved placement of current energy converters subject to environmental constraints,” *International Journal of Sustainable Energy*, pp. 1-15, 2017.
- [24] M. Costa, R. Silva, and J. Vitorino, “Contribuição para o estudo do clima de agitação marítima na costa Portuguesa,” in *Proc. 2as Jornadas Portuguesas de Engenharia Costeira e Portuária*, 2001 (in Portuguese).
- [25] Delft3D-Flow User Manual, 2014.
- [26] G. D. Egbert, and S. Y. Erofeeva, “Efficient Inverse Modeling of Barotropic Ocean Tides,” *Journal of Atmospheric and Oceanic Technology*, vol. 19, pp. 183-204, 2002.
- [27] T. Stallard, T. Feng, and P. K. Stansby, “Experimental study of the mean wake of a tidal stream rotor in a shallow turbulent flow,” *Journal of Fluids and Structures*, vol. 54, pp. 235-246, 2015.
- [28] R. Vennell, “Exceeding the Betz limit with tidal turbines,” *Renewable Energy*, vol. 55, pp. 277-285, 2013.
- [29] T. Stallard, R. Collings, T. Feng, and J. Whelan, “Interactions between tidal turbine wakes: experimental study of a group of three-bladed rotors,” *Phil. Trans. R. Soc. A*, vol. 371, no. 1985, 20120159, 2013.
- [30] A. Forrester, A. Sobester, and A. Keane, *Engineering design via surrogate modelling: a practical guide*. John Wiley & Sons, 2008.
- [31] S. Koziel, and L. Leifsson, *Surrogate-based modeling and optimization: Applications in Engineering*. Springer-Verlag, NY, 2013.
- [32] E. González-Gorbeña, R. Y. Qassim, and P. C. Rosman, “Optimisation of hydrokinetic turbine array layouts via surrogate modelling,” *Renewable Energy*, vol. 93, pp. 45-57, 2016.